Journal of Building Engineering 59 (2022) 105082

Contents lists available at ScienceDirect

Journal of Building Engineering

journal homepage: www.elsevier.com/locate/jobe

Activated sugarcane bagasse ash as efficient admixture in cement-based mortars: Mechanical and durability improvements

Veronica Torres de Sande [a,*], Monower Sadique [a], Ana Bras [a], Paloma Pineda [b]

[a] Built Environment and Sustainable Technologies (BEST) Research Institute, Department of Built Environment, Liverpool John Moores University, Byrom Street, Liverpool, L3 3AF, UK

[b] Department of Building Structures and Geotechnical Engineering. School of Architecture. Universidad de Sevilla, Avda. Reina Mercedes, 2, 41012, Seville, Spain

ARTICLE INFO

Keywords:
Grinding
Waste materials
Biomass ashes
Sugarcane bagasse ash
Sustainability
Low carbon materials

ABSTRACT

Biomass ashes can be used in cementitious materials as cement or sand substitution. Nevertheless, ashes resulted from the combustion of biomass in generation plants present drawbacks that can reduce their potential use if they are not previously treated. In this research, industrial sugarcane bagasse ash (SCBA) was mechanically activated by grinding and its effects evaluated when used as mineral admixture in cementitious materials. Four different substitution rates (0%, 10%, 20% and 30%) where used to investigate the influence of the amount of ashes replaced on the durability and mechanical performance of mortars and identify the optimal substitution rate. To get a thorough comprehension, results were also compared to mortars containing untreated ashes. The combination of a performance-based testing campaign (compressive and flexural strength, open porosity, apparent density, water capillary absorption, surface electrical resistivity, rapid chloride migration coefficient) and a set of analytical techniques (XRD, FT-IR, SEM and TGA-DTA) enabled to characterise the mechanical and durability properties of mortars and identify the mechanisms behind the results. The research concluded that, at 28 days, the incorporation of ground SCBA enhances the compressive strength of mortars up to 62%, decreases the porosity of samples by 35%, highly improves the resistance to the diffusion of chlorides by 10 times and improve the interfacial transition zone by narrowing and closing the gap between aggregates and pastes.

1. Introduction

Nowadays, efforts are put in producing more eco-friendly materials and fostering the circular economy. The research interest lies on i) the increasing high demand of construction materials to meet the needs of the global growing population, ii) the necessity of lowering the carbon emissions of construction industry in specific, and of other waste-producers industries and iii) the social requirement of boosting local resources as a respond to the shortage of raw materials and the consequent increasing in prices.

Building materials and construction sector represents around 11% of all annual global CO_{2eq} emissions. The demand of construction materials will double increase in the years to come as a response to the demands of a global growing population with increasing living standards, and concrete is expected to cover most of the urban development structures. Concrete and cementitious materials production involves a high environmental impact due to i) the increasing global demand, ii) the high emissions of cement production (7% of the world's CO_2 emissions [1]), iii) the water demand that the global production entails and iv) the demand of

* Corresponding author.
E-mail address: v.torresdesande@2018.ljmu.ac.uk (V. Torres de Sande).

https://doi.org/10.1016/j.jobe.2022.105082
Received 26 April 2022; Received in revised form 30 July 2022; Accepted 2 August 2022
Available online 18 August 2022

natural aggregates which extraction is responsible of severe habitat, territory and infrastructures deteriorations and conflicts [2–4]. The world's extracted materials usage will double by 2060, overpassing the 167 Gt [5]. Half of share of non-metallic minerals (the main share of extracted materials) -gravel, sand, clay, limestone, and gypsum, mainly-are used in construction. In parallel, the global biomass production is expected to increase by 68% and the actual global demand of construction materials will double by 2060, overpassing the 86 Gt [5]. Moreover, nowadays, the awareness of returning to the use of local available materials is growing in the population and industry as it poses a strategy to avoid the consequences of raw materials dependency (risks of shortages and market fluctuations) and to reduce the associated transport environmental impact. This entails an opportunity for the built environment to be the driving force in the shift towards more sustainable practices. This, along with the fact that fine aggregates substitution is less investigated, boost and shape this research, that aims to find an outlet for materials that, initially, cannot be used as SCM or cement substituents.

The environmental impact of construction products can be addressed from two complementary points: the production process and the service life of the final product (e.g: reinforced concrete (RC) structure). To reduce the environmental impact of the former, efforts are put in the potential substitution of cement or aggregates by waste materials according to different strategies. These strategies, commonly simultaneous, investigate novel formulations that ensure the extension of service life of the structure, along with lowering the carbon emissions. This is the case of some industrial waste (silica fume, SF; fly ash, FA; ground granulated blast furnace, GGBS) which proved to be beneficial in terms of mechanical and durability performance of concrete and have been already implemented in the production chain. Nevertheless, there are other industrial waste that can be potentially used in construction materials due to their physico-chemical characteristics. Such is the case of ashes resulting from the combustion of biomass in energy plants. The high content in oxides and/or a fineness make biomass ashes attractive to be used as supplementary cementitious materials (SCM). Nevertheless, industrial biomass ashes may show important drawbacks that limit or hinder their use in cementitious material such as: i) a high content in organic matter or undesirable particles as contaminants, salts, porous and light particles; ii) an insufficient content of oxides; iii) a higher water demand due to the increased fineness or higher porosity.

One of these waste is sugarcane bagasse ash (SCBA) which is the resulting material of the combustion of sugarcane bagasse, the most cultivated crop in the world, (1,87 billion tonnes per year [6]). On the yield basis, the annual SCBA production is estimated in 48–60 million of tonnes [7] entailing an environmental problem if they are dumped. Traditionally, it has been used as fertilizer, although the nutrient capacity of ashes has been put into question [8] and its potential risks due to the heavy metal and other contaminants content highlighted, compromising the use of ashes as fertilizer [9].

SCBA has been investigated as cement replacement since it usually presents proper chemical composition to be used as artificial pozzolan (high content of amorphous silicon). Nevertheless, the oxides content (SiO_2, Al_2O_3 and Fe_2O_3, hereafter S-A-F) does not always fall within the standard threshold of 70% content [10] stablished by BS EN 450–1:2012 [10] for a similar material (coal fly ash with or without co-combustion materials) already incorporated as pozzolan to be used in concrete. In addition, the quality of industrial ashes is commonly compromised due to the high temperatures and uncontrolled conditions during the combustion process. Thereupon industrial SCBA may not exhibit a desirable amorphous portion, loss on ignition (LOI) content and can contain additional contaminants that compromise the workability, chemical reactions, soundness, and durability of the material.

Much research focused on Ordinary Portland cement (OPC) as a strategy to reduce the emissions of its production. In terms of mechanical performance has been declared to be 15–20% (weight of cement) for ultra-treated ashes in mortars and concretes [11–13] and between 5 and 10% for untreated or low-treated ashes [14,15]. The substitution of cement is limited due to the dilution effect which entails a lower initial hydraulic reactivity due to the absence of cement. Few authors have addressed the use of industrial SCBA as sand substituent, although the optimal substitution rate does not seem to be clear. Sales and Lima [8] investigated the substitution of sand by poor-reactive untreated SCBA with different type of cement and found that higher amounts of ashes (20–30% in mortars and up to 50% in concrete) could be used delivering higher compressive strength values after 28d. Contrary, Modani and Vyawahare [16] substituted up to 40% of untreated fine aggregates (weight of sand) in concrete and observed that substitution rates, SR, higher than 10% resulted in the reduction in the compressive strength along with the increasing rate of ashes at 28d. The CS loss at 20% SR was considered negligible in terms of CS and workability. Macedo et al. [17] concluded that 10% of fine aggregates substitution delivered the highest compressive strength in mortars being 3% the optimal substitution rate if tensile strength is considered. In general, SBCA benefits the durability performance of cementitious materials regardless the gain or not in the compressive strength [7,13,18–20]. The variability in the results mainly lies on the wide casuistry used in terms of mix designs, the wide range of characteristics of the raw material and the processed material.

In this research, industrial SCBA with a portion of oxidising matter (organic carbon) above 5%, a content in oxides (S-A-F) lower than 70% and a strength activity index below 75% has been used in the production of mortars. These ashes previously demonstrated that can benefit chlorides penetration resistance of OPC systems when used as mineral admixture substituting fine aggregates [7]. Contrary, the ashes, which were sieved, and the portion retained in the 212 μm sieve removed, dramatically reduced the flowability, increased the open porosity and diminished the compressive strength at 28 days in comparison to the control samples. A retarded pozzolanic reaction was observed within the mixes containing SCBA. In the current investigation the effectiveness of the physical and mineralogical activation by grinding is investigated in an attempt to encounter the potential drawbacks that untreated ashes may represent. The effectiveness of grinding lies on the increase of fineness of SCBA promoting the filling effect and on the exposition of more surface area of particles for pozzolanic reaction [21]. Fillers create extra nucleation sites for the formation of more hydration products. Grinding of supplementary cementitious materials is known to increase the workability and the pozzolanicity and, therefore, the compressive strength [22,23]. Cordeiro et al. [23] correlated the increase in compressive strength of mortars containing ground SCBA and the increase in the packing density, and the increase in pozzolanicity (Chapelle activity) and the fineness. Nevertheless, grinding of sugarcane bagasse seems to not be effective until achieving certain fineness (<60 μm) [19,21,24]. Thus, the benefits of

Table 1
Chemical data of ashes, sand, and cement.

		Main Oxides											pH	$\%_{amorphous}$	SAI %
	CaO	SiO_2	Al_2O_3	Fe_2O_3	S + A + F	MgO	K_2O	TiO_2	Na_2O	MnO	Cl^-_{ws}	SO_3			
Ut-SCBA	13.08	48.08	6.07	5.92	**60.07**	2.42	2.10	0.55	1.34	0.13	0.18	0.96	12.56	80.7	51%
G-SCBA	13.90	53.17	7.11	6.01	**66.29**	2.67	2.24	0.525	1.31	0.14	0.24	0.85	12.97	81.2	73%
Sand	0.29	76.45	3.21	0.27	–	0.81	0.70	0.05	–	0.00	–	0.14	–	–	–
Cement	76.56	18.68	3.25	3.11	25.04	1.82	0.86	0.25	–	0.55	–	2.60	–	–	–

ws: water soluble, Tot: total content, considered to be the acid soluble content.

Table 2
Physical data of ashes, sand, and cement.

	Particle size distribution						Real density (kg/m^3)	Bulk density (kg/m^3)	SSA (m^2/kg)
	Mean μm	Median μm	D_{10} μm	D_{50} μm	D_{75} μm	D_{90} μm			
Ut-SCBA	221	131	25.5	130.8	264.7	613.8	2449	718	442.8
G-SCBA	19.5	10.4	1.5	10.4	25.3	50.5	2551	928	817.1
Sand	333	296	198	296	373.3	476	2420	1635	36.0
Cement	19.1	15.3	2.2	15.3	26.7	39.6	3150	1400	163.5

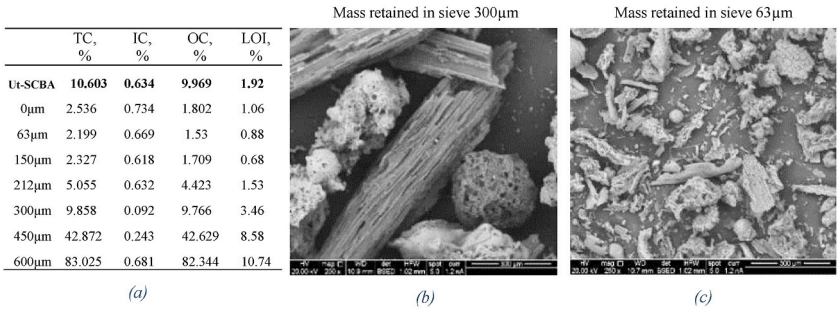

Fig. 1. Characterisation of Ut-ashes by size. (a) TC, IC, OC and LOI values, (b) Mass retained in sieve sizing 300 μm and (c) mass retained in sieve sizing 63 μm.

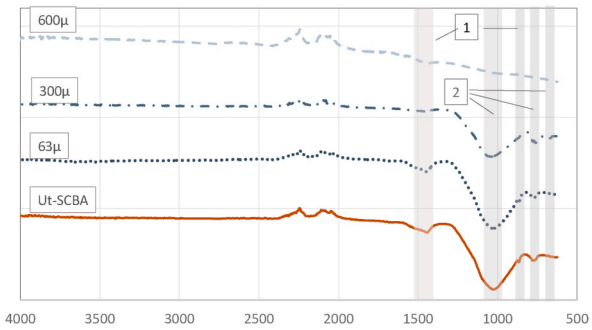

Fig. 2. FT-IR of Ut-SCBA. Identification of (1) group carbonate CO_3^2 and (2) vibrations of the bonds Si–O of quartz.

grinding might be hindered by the high presence of crystalline particles (quartz and cristobalite) and carbon content. The crystallinity if demonstrated to be high, can be counteracted by ultra-grinding leading to more nucleation sites able to form more hydration products.

In this research four different substitution rates (0%, 10%, 20% and 30%) where used to investigate the influence of the amount SCBA used as mineral admixture on the durability and mechanical performance of OPC systems (mortars and pastes) and identify the optimal one. To get a thorough comprehension, results were also compared to mortars containing untreated ashes. The combination of a performance-based testing campaign (compressive and flexural strength, open porosity, apparent density, water capillary absorption, surface electrical resistivity, rapid chloride migration coefficient) and a set of analytical techniques (XRD, FT-IR, SEM and TGA-DTA) enabled to characterise the mechanical and durability properties of mortars and identify the mechanisms behind the results.

2. Materials and methods

2.1. Materials

2.1.1. Cement and sand

To produce the mortar samples, cement type CEMI 52.5 N from HANSON and local available commercial sand were used. Physicochemical characteristics are shown in Table 1 and Table 2.

2.1.2. Untreated sugarcane bagasse ash, Ut-SCBA and ground sugarcane bagasse ash, G-SCBA

Industrial SCBA was collected from the 30Mw San Pedro Bio Energy plant in Dominican Republic. The ashes were the result of the combustion of bagasse at 750-800 °C. The system used is based on a travelling grate boiler were the resulting ashes of the combustion of the bagasse is retained in filters. Untreated (Ut-SCBA) and ground ashes (G-SCBA) were used in this research. G-SCBA was obtained

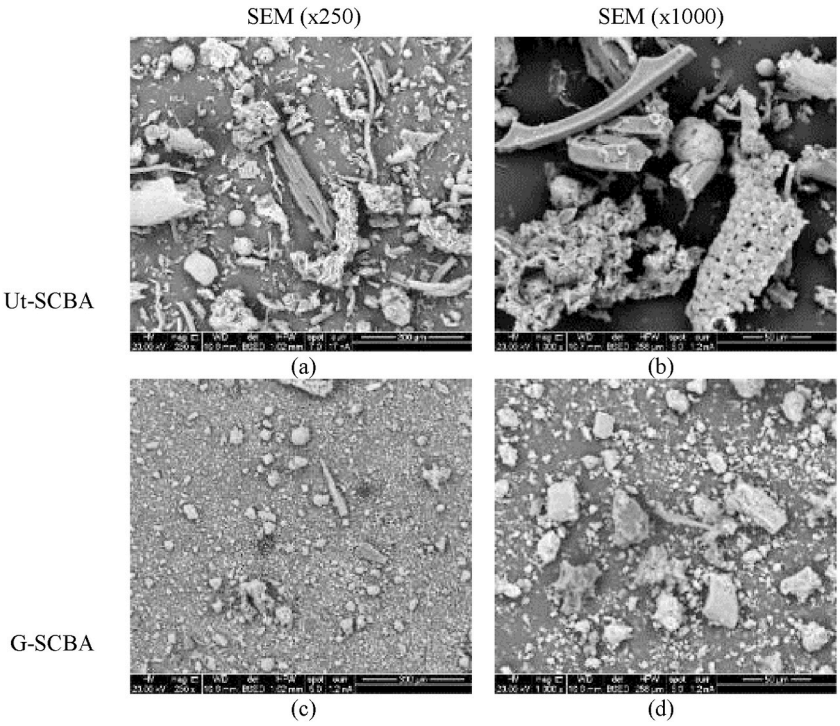

Fig. 3. SEM images of Ut-SCBA and G-SCBA.

by using a mortar grinder, model Retsch RM 200 in constant-mass portions until getting $D_{75} \sim 25$ μm. The chemical composition and physical properties of untreated and treated ashes are provided in Tables 1 and 2.

The appearance of Ut-SCBA, with grey colour and black char particles, confirms the uncompleted combustion of the biomass, Fig. 1 (b). This, along with its heterogeneous composition, influence the fresh and hardened properties of mortars. By means of SEM, particles sized below 212 μm are rich in alumina and silicon, presenting a wide range of shapes. According to the XRD pattern, the 212 μm portion has a larger hump corresponding to the presence of amorphous compounds [25]. Particles above 300 μm are comprised by light oval or elongated carbonaceous particles and crystalline $CaCO_2$ and SiO_2 (the latter corresponding to particles dragged from the field during the harvesting the biomass), Fig. 2. The organic carbon (OC) particles presence increases with the increase of particle sizing, meanwhile the inorganic carbon (IC), in minor presence, decrease, Fig. 1. Therefore, commonly, the portion above 150 μm [26] is removed as a basic treatment, which, in this research, entails the 18% of the total mass.

The determination of LOI in accordance with BS 196–2 [27], method for testing cement, is widely used in the characterisation of waste materials that are meant to be used as SCM, since its content is limited by standards as per BS EN 450–1:2012 [10]. In LOI the carbon dioxide and water are eliminated and any oxidable elements oxidised to some extent. Nevertheless, the use of LOI test has been put into question since overestimations may occur due to further chemical reactions at different temperatures [9,28]. In this research, however, it was found that this method is inefficient in completely combusting the carbonaceous particles due to the size and the pre-carbonation state of particles, therefore is not suitable for testing biomass ashes Fig. 1(a). By using a carbon content analyser and thermogravimetric analysis with the same range of temperature, the results were 9.97% (OC) and 8.25%, respectively. On the other hand, the weight loss in the range associated with the carbon decomposition (400°C–650 °C) in TG analysis is of 3.42%.

XRD results reveal that the main crystalline phases are quartz (SiO_2), calcite ($CaCO_3$), akermanite ($Ca_2MgSi_2O_7$), mullite ($Al(Al_{1.272}Si_{0.728}O_{4.864})$), moissanite-3C (SiC) and anorthite $Ca(Al_2Si_2O_8)$. Sugarcane bagasse ashes are rich in SiO_2 (48.08%), followed by CaO (13.08%), Al_2O_3 (6.07%) and Fe_2O_3 (5.92%), Table 1. The sum of SiO_2, Al_2O_3 and Fe_2O_3 entails the 60.07%, below the minimum (70%) required by BS EN 450–1:2012 [10].

All FT-IR spectra showed bands of the group carbonate CO_3^2, in the ranges of 1446 cm^{-1} and 882 cm^{-1} with higher absorption bands for portions below 150μ. This corresponds to the presence of calcium carbonate, potentially due to the reaction of calcium hydroxide with the environmental CO_2. Vibrations of the bonds Si–O of the quartz at 1150 cm^{-1} were observed in all retained portions but in 600 μm, with higher absorption bands for finer particles that attributed to amorphous silica. Secondary silicon structures are shown at 798 and 670 cm^{-1} with higher intensity in the mass retained in sieve 212μ, corresponding to crystalline silica of sand (quartz) as observed in SEM. In addition, vibrations of the group Al–O might be covered by the presence of silicon in the range of 882 and 928 cm^{-1}.

Grinding leads to the breakdown of porous and crystalline particles, therefore to the homogenisation of the material. The different grindability of particles [29] explains the major presence of crystalline particles in bigger sizes, Fig. 3. Grinding additionally increases the real density until that of sand and rise the SSA by five times similar to that of cement, Table 2. During the morphology investigation by means of SEM, entrapped particles in porous structures were observed, and might be behind the increase in S + A + F oxides

Table 3
Mortar and pastes mix design.

	Treatment	SR	CEM (kg)	Fine aggregate (kg)		w/b	w/c
		%		Sand	Ash		
Control	–	0	1	3	–	0.500	0.500
Ut_{20}	Untreated	20	1	2.4	0.6	0.525	0.840
G_{10}	Ground	10	1	2.7	0.3	0.387	0.504
G_{20}	Ground	20	1	2.4	0.6	0.346	0.550
G_{30}	Ground	30	1	2.1	0.9	0.339	0.644

(66.29%) after been released by the breakdown of the retaining particle.

The percentage of the amorphous portion is a qualitative measure obtained by integrating the area below the line in the XRD graph. According to the XRD results, the amorphous portion of Ut-SCBA and G-SCBA are equivalent. However, the strength activity index, SAI, of Ut-SCBA (59%) is far from that of G-SCBA (73%) which is comparable, but still lower, to the minimum required (75%) by BS EN 450–1 [10] pozzolans to be used in concrete, mortar and grouts. Differences between both methods can be attributed to the different particle size of the sample that influences the readings. The sum of silicon dioxide, aluminium oxide and iron oxide (S + A + F) is lower that the limit (70%) stipulated in the same standard [10], Table 1. This standard was observed due to the similarities between fly ash (pulverised coal fly ash with or without co-combustion materials) and SCBA.

Therefore, this, along with the fact that fine aggregates substitution is less investigated, boost and shape this research, that aims to find an outlet for materials that, initially, cannot be used in cement substitution.

2.2. Methods

The methods used are divided in three subsections as follows:

2.2.1. Characterisation of raw materials

Physico-chemical properties of raw materials were investigated. The morphology was observed by means of scanning electron microscope (SEM) using FEI SEM model Inspect S50, and the elemental composition of particles obtained by coupling an energy dispersive X-Ray spectroscopy (EDS). The particle size distribution of samples (PSD) was obtained by means of laser diffractometry test using a Beckman Coulter LS13320 analyser as per BS ISO 13320–1:2009 [30]. These results must be interpret as apparent PSD since the method makes an approximation for non-spherical particles as observed before in [7] Bulk density, real density and specific surface area (SSA) based on the Blaine fineness method were obtained as per BS EN 1097–6:2013 [31] and BS EN 196–6:2018 [32]. Real density was measured with a helium Quantachrome multipycnometer. The elemental composition of raw materials was determined by using a Shimadzu EDX 720, energy dispersive X-ray fluorescence (EDXRF) spectrometer, and water-soluble chlorides and sulfates analysed by using a spectrophotometer DR3900 from HATCH. Phases were determined by using an X-ray diffractometer type Miniflex RIGAKU with CuK X-ray radiation (40 kV voltage and 15 mA current at scanning speed of 5.0 deg./min in continuous scan mode) and scanning range (2θ) of 3–90°. Fourier transform infrared spectroscopy (FT-IR) analysis was carried out to characterise the raw materials and identify the different hydration products in pastes by using an Agilent Technologies Cary 630 FTIR with a diamond crystal. The spectrum of the sample was recorded using accumulating 16 scans over a 4000 cm^{-1} and 650 cm^{-1} wavelength range. Loss on ignition (LOI) was obtained as per BS EN 196–2:2013 [27]. Additionally, a Primacs 100 analyser based on Dumas chemical combustion method was used to determine the Total Carbon (TC), Inorganic Carbon (IC) and Total Organic Carbon (TOC). Thermogravimetric analyses (TG) to determine weight loss of the material subjected to thermal changes and differential thermal analysis (DTA) -first derivative of TG-to detect phase changes were carried out with a PerkinElmer TA-Q50 analyser V20.13 Build 39. The heating range covered 20-1000 °C by applying a heating rate of 10 °C/min.

2.2.2. Mix design, preparation and curing of mortars and pastes

Cementitious mortars were prepared by using four different substitution rates (SR), 0%, 10%, 20% and 30%, by weight of fine aggregate. These samples were labelled as Con, $G_{10,}$ G_{20} and G_{30} respectively. To compare the effectiveness of the treatment a set of mortars containing Ut-SCBA was casted. For this purpose, 20% of SR was selected based on its optimal performance at 28 days. Additionally, pastes were prepared to investigate the microstructure and mineralogical composition. To simplify the paper, all the results (Control, Ut_{20}, G_{10}, G_{20} and G_{30}) are shown together. A batch of 160x40 × 40mm mortar prisms and 100 × 200mm mortar cylinders were casted per composition. Three prisms and two cylinders were manufactured for each age and composition, making a total amount of 15 prisms and 10 cylinders per composition and 75 prisms and 50 cylinders in total. Cylinders were further cut in 50 mm heigh specimens. Mortars were designed as per British Standard 196–1 [33], with a cement to aggregate ratio 1:3, water to binder ratio (w/b, in which binder is considered to be the sum of the amount of cement and ash) such that it equals the flow value of the control sample (116±3 mm), with a water to cement ratio (w/c) of 0.5. Ut-SCBA or G-SCBA were added in substitution of a controlled percentage (described in section 2.1) of weight of fine aggregates as per Table 3. Additionally, pastes were prepared, by maintaining the proportions derived from the mortar composition, removing the portion of sand. In the case of control pastes, due to the high excess of water, the w/b ratio was reduced to the standard consistency value that equals 0.27.

Mortars and pastes were constantly cured in tap water at laboratory conditions until the specific testing date.

Table 4
Performance-based tests.

Physical and chemical properties	Abbreviation	Tests	Age (days)
Consistence of mortars (Flow test)	–	BS EN 1015–3 [34]	0
Density of fresh mortar	D_f	BS EN 1015–6 [35]	0
Apparent density of hardened mortar	D_{app}	BS EN 1936: 2006 [36]	3, 7, 28, 56, 90
Compressive strength	CS	BS EN 196–1:2016 [33].	3, 7, 28, 56, 90
Flexural strength	FS	BS EN 196–1:2016 [33].	3, 7, 28, 56, 90
Capillary water absorption	CA	BS EN 1015–18:2002 [37]	3, 7, 28, 56
Total open porosity	OP	BS EN 1936: 2006 [36]	3, 7, 28, 56, 90
Rapid chloride migration test	RCMT	NT Build 492 [38]	7, 28, 56, 90
Surface electrical resistivity	ρ_{sur}	Wenner four-probe system	3, 7, 28, 42, 56, 90

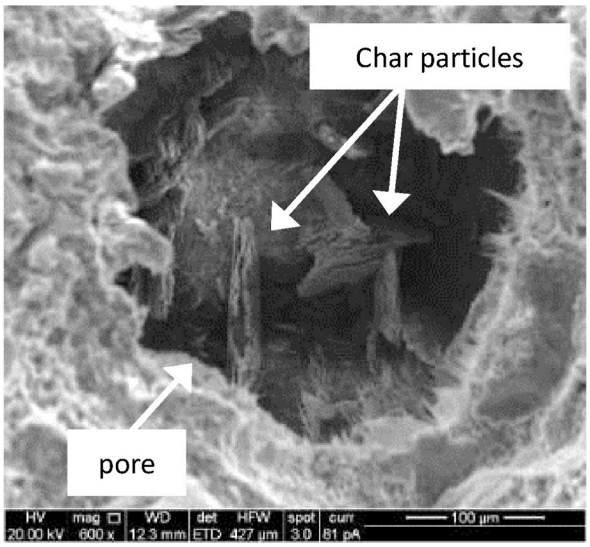

Fig. 4. Pore of Ut-paste at 28d observed by means of SEM.

2.2.3. *Characterisation of mortars and pastes*

The experimental campaign combines a selection of performance-based tests and analytical techniques. The performance-based tests were selected to investigate the fresh and hardened state. Standards and age of curing at the time of testing are summarised in Table 4.

Mechanical performance was covered by compressive (CS) and flexural strength (FS) tests. The durability performance assessment focusses on chloride attack related tests because of its major role in service life reduction of reinforced concrete infrastructures. Therefore, rapid chloride migration test (RCMT) and surface electrical resistivity (ρ_{sur}) were carried out to assess the resistance of mortars against chloride penetration. Additionally, the latter is used to indirectly track the hydration of mixes. Open porosity (OP) and apparent density (D_{app}) of hardened specimens were obtained at different ages and correlated with the mechanical and durability results.

Additionally, a combination of analytical techniques based on different operational principles were done to get a thorough information of the formed hydration products and investigate and confirm the mechanisms behind the results obtained in the performance-based tests [39]. These techniques were XRD, FT-IR, SEM and TG-DTA and the main points of interest were: i) the formation and identification of hydration products, ii) the correlation of hydration products to the results observed in the mechanical and durability performance of mortars, ii) the identification and track of particularised changes during the hydration process in the matrix due to the addition of SCBA, iii) the identification of changes attributable to the mechanical activation.

Superficial electrical resistivity (ρ_{sur}) test has been used to indirectly measure the electrical resistivity of mortars [40], a material property that measures the opposition of the mortar mass to the transport of charged ions through the material under an external current [41]. Three readings of electrical resistance were taken weekly with a Wenner probe on each cylinder (length: 200 mm, Ø:100 mm), in saturated conditions. The electrical resistance was then converted into resistivity as per [42] by applying a cell constant correction, $k = 2.63$, for small bodies.

The interfacial transition zone (ITZ) between aggregates and cementitious paste, known to be an heterogeneous, weak and porous zone, was investigated in all mortars at 28 and 56d by means of SEM. To facilitate the investigation of the ITZ, the images obtained were subsequently photograpically treated in such a way that the porous and gaps were highlighted in black. Same parameters were applied to all images.

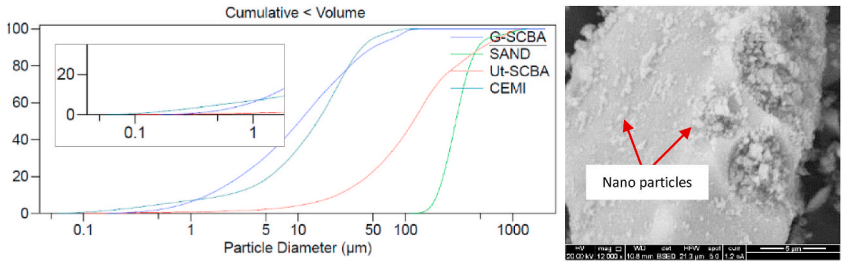

Fig. 5. Particles sizing below 1 µm provided by G-SCBA.

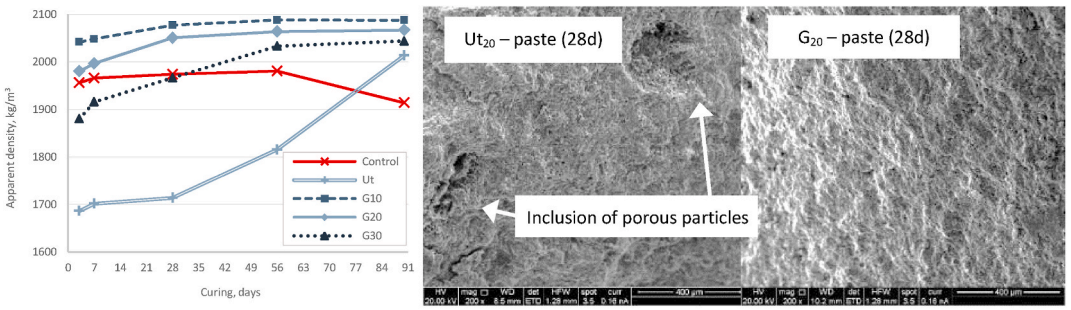

Fig. 6. Hardened apparent density of mortars (a), SEM of Ut20 paste (b) and G20 paste (c) at 28d.

3. Results and discussion

3.1. Influence of grinding in fresh properties of mortars

Water to binder ratio (w/b), considering 'binder' as the sum of cement and ashes, was adjusted for each composition to get the same flow value obtained for the control samples (116±3 mm), Table 3. The substitution of sand by untreated biomass ashes increases the water demand due to a higher porosity, higher SSA or for not being totally inert. Ut-SCBA increases the water demand per cubic metre of mortar by a 68%. Additionally, it was observed a bleeding effect where an excess of water retained by the porous particles during the mixing time was released, giving rise to the formation of a more porous structure. This has been corroborated by means of SEM where pores appear around the concentration of char particles, Fig. 4.

On the contrary, when G-SCBA is used, the water demand is reduced by a 40%–23.3% in comparison to Ut-SCBA by breaking down the porous structures. This is particularly important since waste materials commonly increase the water demand. However, when compared to control specimens, despite lowering the w/b ratio along with the amount substituted, G-SCBA raises the total water demand by 0.8%, 10.0% and 28.8%. Contrary to the capacity of ground ashes to increase the flowability of mortars, in terms of consistency, it was also observed that these increase the plastic viscosity along with the amount of sand substituted. These two observations can be explained by the hypothesis that G-SCBA increases the portion of nano particles (particles sizing below 1 µm) which lowers the amount of lubricating water available within the interparticle voids, leading to the increase of the yield stress and plastic viscosity of mortars [43] (see Fig. 5).

3.2. Influence of grinding in hardened properties of mortars

3.2.1. Apparent density

Apparent density (ρ_b) of hardened mortars is affected by the substitution of sand by ashes. Ut-SCBA reduces the bulk wet density of mortars by 12.8% at 28d. This reduction results from the use of additional amount of water (Table 3), the consequent more porous structure (Fig. 4) and the inclusion of lighter and more porous particles in the matrix, sizing up to 300µ −600µ. Nevertheless, the gain in density highly increases between 28 and 90d due to a delayed pozzolanic reaction, overpassing the control one after 56d. In contrast to Ut-SCBA, the use of G-SCBA increases the density of mortars for substitution rates of 10% and 20% achieving relative gains at 28d of 5.6% and 4.3%, respectively, Fig. 6. The higher the G-SCBA substitution rate, the lower the apparent density at early ages, but the higher the absolute gain in density. This is the case of G_{30} which does not achieve the control's apparent density until 28d but shows the steepest gain in density. The reasons for the increases in apparent density when ashes are ground lie in i) the breaking down the big light and porous particles, ii) the densification of the pore structure due to the filling effect of finer particles, and iii) the refinement of the matrix by the formation of secondary CSH gel. The former was proved by the apparent density development over time, Fig. 6 (a). It is worth noting that the major enhancement (19.4%) in terms of apparent density occurs in mixes blended with untreated ashes, in contrast to G_{10}, G_{20} and G_{30} mixes (4.34%, 1.2%, 7.98%, respectively). This contrasts with the CS results. The lower CS values of Ut-mixes regardless the apparent density values can be explained due to i) the existence of bigger isolated porous as a result of the

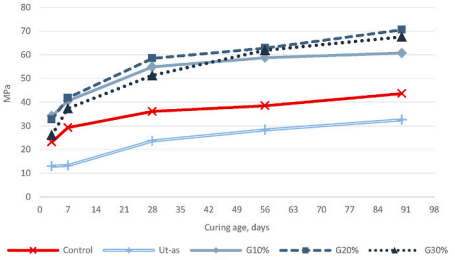

(a)

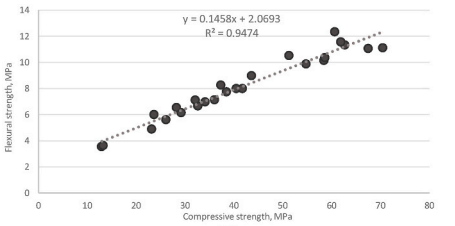

(b)

	Age days	FS MPa	CS MPa	FS/CS	CS/ρ_b
Con	3	4.88	23.20	0.210	0.0119
	7	6.14	29.28	0.210	0.0149
	28	7.13	36.06	0.198	0.0183
	56	7.73	38.50	0.201	0.0194
	90	8.98	43.64	0.206	0.0228
Ut	3	3.54	12.97	0.273	0.0077
	7	3.63	13.27	0.274	0.0078
	28	6.00	23.69	0.253	0.0138
	56	6.54	28.30	0.231	0.0156
	90	7.10	32.11	0.221	0.0159
G10	3	6.96	34.14	0.204	0.0167
	7	7.99	40.53	0.197	0.0198
	28	9.87	54.83	0.180	0.0264
	56	10.36	58.67	0.177	0.0281
	90	12.33	60.66	0.203	0.0291
G20	3	6.66	32.68	0.204	0.0165
	7	7.99	41.79	0.191	0.0209
	28	10.15	58.46	0.174	0.0285
	56	11.13	60.31	0.185	0.0292
	90	11.11	70.52	0.158	0.0341
G30	3	5.60	26.15	0.214	0.0139
	7	8.25	37.37	0.221	0.0195
	28	10.52	51.30	0.205	0.0261
	56	11.55	61.90	0.187	0.0305
	90	11.06	67.53	0.164	0.0330

(c)

Fig. 7. Compressive strength evolution, MPa (a), FS to CS ratio (b), numerical data (c).

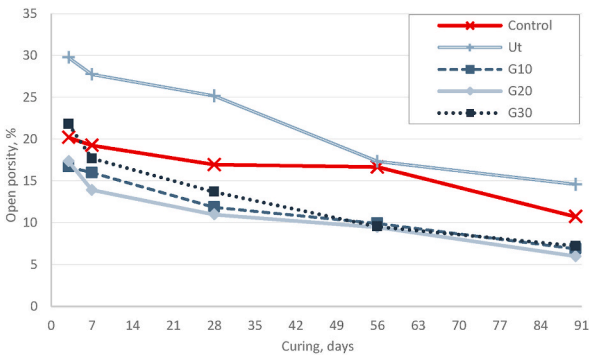

Fig. 8. Open porosity of mortars at 3, 7, 28, 56 and 90 days.

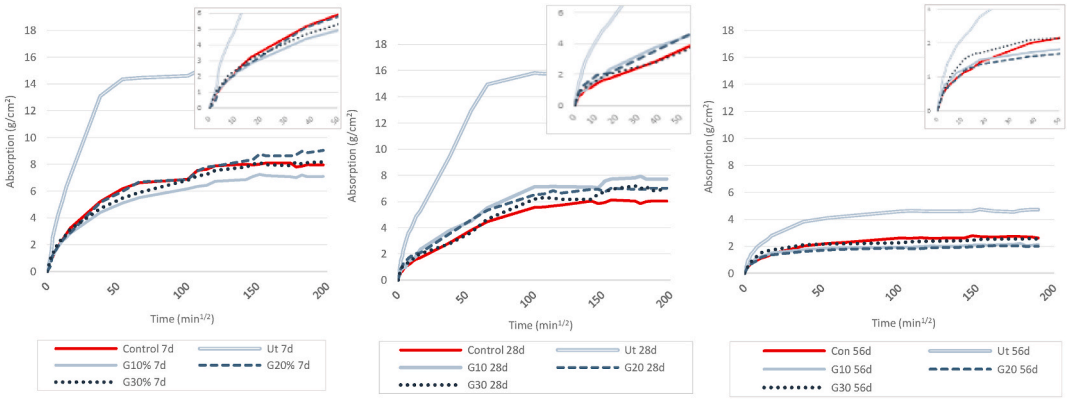

(a) (b) (c)

Fig. 9. Capillary absorption of mortars at 7d, 28d and 56d

pozzolanic reaction, ii) the inclusion of porous structures that, in the case of G-mixes are broken, Fig. 6 (b), and iii) the weaker ITZ formed, Fig. 16.

When compressive strength and apparent density are correlated, Fig. 7c, it can be observed that the CS/ρ_b ratio is higher for G-SCBA

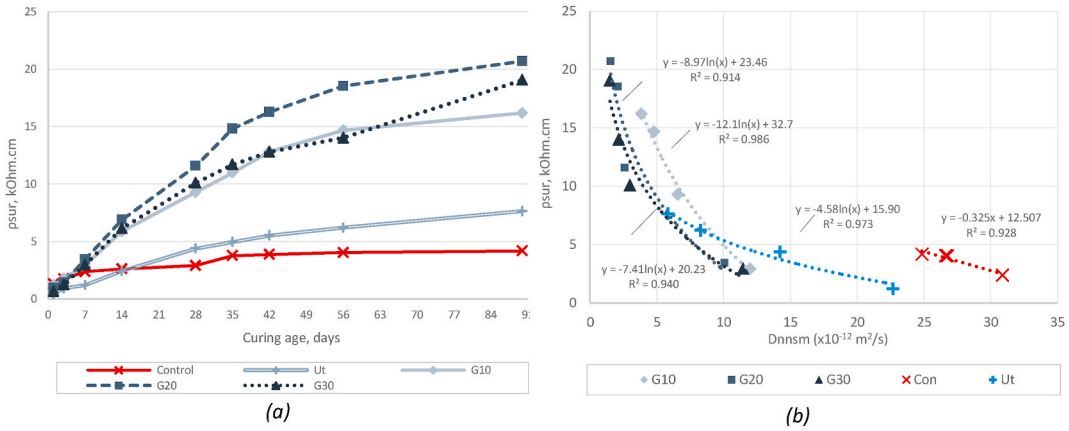

Fig. 10. (a) Surface Electrical Resistivity and (b) correlations between surface electrical resistivity and RCMT.

mixes. This can be interpreted as the major capacity of ground ashes to promote the production of CSH gel by the facilitation of more nucleation sites [44], blocking the microstructure channels and creating isolated pores and therefore, reducing the open porosity and the apparent density.

3.3. Mechanical properties

Ut-SCBA decreases the compressive strength (CS) and flexural strength (FS) of mortars up to 52,2% and 15,4%, respectively, at 28d due to the higher amount of water and char particles resulting in a more porous and weaker matrix. This agrees with the results analysed later in terms of porosity and capillary absorption, Fig. 8 and Fig. 9. Contrary, the addition of G-SCBA highly increases the CS and FS of mortars. In G_{10} and G_{20} mixes increments of 38% and 42% in comparison to control samples are achieved, respectively, at early ages (3–7days), although the highest CS gains, 52% and 62% respectively, take place between 7 and 28 days. On the other hand, G_{30} compressive strength is comparable to that of the control mixes at 3 days and shows a constant strength gain on time overpassing G_{10} and G_{20} CS after 56 days. The results show that the finer particles obtained by grinding enhanced the mechanical performance of mortars at early ages in comparison to untreated ashes by increasing the packing density which is directly proportional to the compressive strength [23]. Subsequently, untreated and ground ashes promote the pozzolanic activity by the consumption of portlandite in pursuit of the creation of secondary CSH gel. Additionally, the outstanding performance of mixes containing G-SCBA in comparison to Ut-SCBA may lies in the creation of more nucleation sites [44]. Gains in CS are observed up to 90 days.

In terms of flexural strength (FS), it exists a linear trend regardless the composition, Fig. 7b. When the flexural to compressive strength ratio is analysed, the most significant observation is the fact that FS/CS is higher for Ut-mixes what can be explained due to the participation of preferential char fibres in the FS, observed when breaking the samples. However, this should be deeply investigated. In addition, for G_{20} and G_{30} mixes, the ratio decreases on time highlighting the main participation of the delayed pozzolanic reaction on the CS.

3.4. Durability properties

3.4.1. Open porosity

The addition of Ut-SCBA induces increments above 47% in open porosity (OP) of mortars until 28d. Between 28 and 56d, OP is highly decreased until achieving that of the control samples. A delayed pozzolanic reaction is behind of this improvement, when the consumption of portlandite to produce secondary CSH gel, results in the densification of the matrix. This agrees with the results observed in terms of compressive strength and electrical resistivity, Figs. 7 and 10. Although according to these tests, the process would be boosted between 7 and 28d. Contrary, the capillary absorption is much higher than the control samples even after 28d.

The addition of G-SCBA decreases the OP in all cases, except for G_{30} mixes at 3d, which is, in any case, on the range of the control samples. The higher amount of ground ashes is used, the lower the reduction in OP at early ages, but the higher the reduction over time until stabilisation at 56d when all G-samples achieved similar OP ($\simeq$10%), resulting in reductions above the 40% in comparison to the control samples. Reductions continue up to 90d with no clear differences between G_{10}, G_{20} and G_{30}.

3.4.2. Capillary water absorption

Capillary water absorption measures the water entering by capillary action from the saturated external surface throw the pores of the mass due to the exitance of surface tension without any external action. Therefore, the action is limited by definition, achieving the equilibrium after a period of time if the environmental conditions are maintained.

As plot in Fig. 9, grinding highly promotes the refinement of the pore structure in comparison to untreated ashes achieving that of the control samples since early ages. At 56d, G_{10}, G_{20} and G_{30} specimens outperform the performance of control specimens by 11.9%, 18.6% and 2.3% after 48h, while Ut-SCBA steep fall off as pointed for OP. No major differences are observed in terms of substitution rate for G-specimens. The reach of the plato forwards along with the curing age, reducing from 14d to 10d and 7d at 7d, 28d and 56d, respectively. These observations are in agreement with the normal hydration evolution. Nevertheless, the reductions in terms of OP

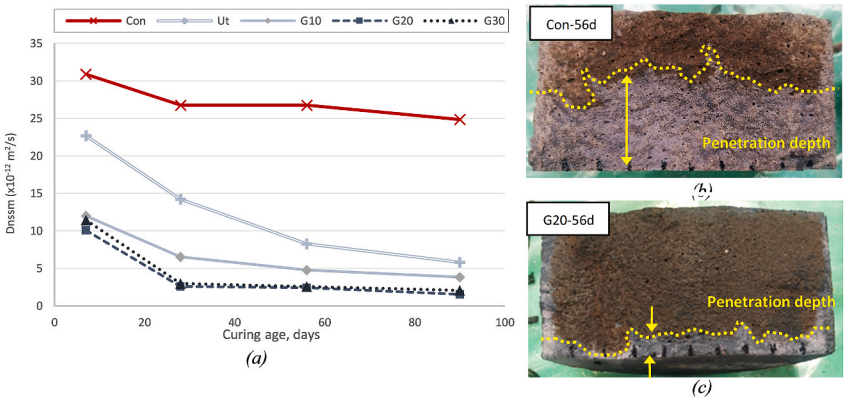

Fig. 11. (a) Chloride migration coefficient at 7d, 28d,56d and 90d; and specimens Con-56d (b) and G20-56d (c).

were more significant than those observed for G-specimens and G_{30} in specific. Moreover, the non-steady state chloride migration coefficients are much lower for blended mixes regardless the treatment. Consequently, it can be concluded that this test should not be used by its own to assess the risk of aggressive agent attack in cementitious materials containing SCMs.

3.4.3. *Electrical resistivity, ρ_{sur}*

ρ_{sur} of control specimens increases until 28-35d up to 3.76kOhm.cm and then keeps almost constant with minor gains; this can be correlated to the normal hydration processes of OPC materials. Adding SCBA to the mortar mixes abruptly increases the ρ_{sur} of specimens containing G-SCBA and Ut-SCBA after 7d and 14d, respectively. Ut-SCBA improves the ρ_{sur} of control samples by 51% after 28d and 83% at 90d. On the other hand, G-SCBA sharply increases the ρ_{sur} of mortars by 220%, 298% and 248%, for G_{10}, G_{20} and G_{30} mixes at 28d and by 288%, 395% and 357% at 90d.

The constant increases observed on the electrical resistivity denote a reduction on the permeability due to the refinement and blockage of the pore's microstructure over time that, in both cases, treated and untreated ashes, correspond to the formation of secondary CSH and CASH gel. CSH and CASH gel formation was also observed by means of SEM and XRD at different ages, Fig. 12. This is in agreement with the reductions and improvements observed in open porosity and in the mechanical performance, respectively. Therefore, it is demonstrated that low reactive Ut-SCBA partially promotes the formation of CSH, which is accelerated and highly increased by mechanical activation.

There is a log-based correlation between surface electrical resistivity and RCMT coefficients for mixes containing ashes ($R^2 \geq 0.90$), Fig. 10. Instead, due to the short enhancement in samples with no addition of SCBA in any form (control) a linear equation can describe the relation between the two characteristics.

3.4.4. *Non-steady state migration coefficient, D_{nssm}*

Rapid Chloride Migration test (RCMT) is a rapid experiment to measure the time it takes for chloride ions to diffuse into concrete. The addition of untreated ashes reduces the non-steady state migration coefficient (D_{nssm}) of control samples by 26.6%, 46.5% and 69% and 76.8% at 7d, 28d, 56d and 90d despite the higher porosity of the former, Fig. 11. This fact demonstrates that the beneficial influence of SCBA on the durability properties does not only lie on the densification of the matrix but potentially on the morphology and tortuosity of the pores structure that will be in agreement with the complex and heterogeneous matrix observed in Ut-specimens, Fig. 16(b1).

In G-SCBA blended compositions, major improvements in comparison to the control samples are observed as follows, Fig. 11: $G_{10\text{-}7d} = 61\%$, $G_{10\text{-}28d} = 75\%$, $G_{10\text{-}56d} = 82\%$, $G_{10\text{-}90d} = 85\%$, $G_{20\text{-}7d} = 67\%$, $G_{20\text{-}28d} = 90\%$, $G_{20\text{-}56d} = 92\%$, $G_{20\text{-}90d} = 94\%$, $G_{30\text{-}7d} = 63\%$, $G_{30\text{-}28d} = 89\%$, $G_{30\text{-}56d} = 92\%$, $G_{30\text{-}90d} = 94\%$. Therefore, the use of SCBA enhances the chloride penetration resistance of the matrix regardless the treatment and the SR. Nevertheless, the results obtained depict different probably mechanisms and an apparent limit. Hence, Ut-specimens shows the major evolution. It also calls the attention the more horizontal trend of the curve that correlates the surface electrical resistivity and the non-steady state diffusion coefficient from RCMT of Ut-specimens.

3.5. *Influence of grinding in mineralogical structure of mortars*

The formation and identification of hydrates were tracked by means of XRD, FT-IR and TGA-DTA. Emphasis was placed in highlighting those attributable to the addition of SCBA and in specific to the mechanical activation.

3.5.1. *XRD*

Fig. 12 shows the diffraction pattern of pastes at 7, 14, 28, 56 and 90 days of curing. By comparing the patterns at different ages the different hydration products kinetics can be analysed in their crystalline forms. The main change is the one that affects the portlandite, CH ($Ca(OH)_2$) and CSH gel. In control samples CH continues forming over time as per CSH. On the other hand, in blended pastes CH decreases while crystalline calcium silicate hydrates (CSH) and calcium aluminate silicate hydrates (CASH) increases as a result of the formation of the latter through the consumption of the former. There is a major presence of CH in Ut_{20} than in G_{20} pastes confirming

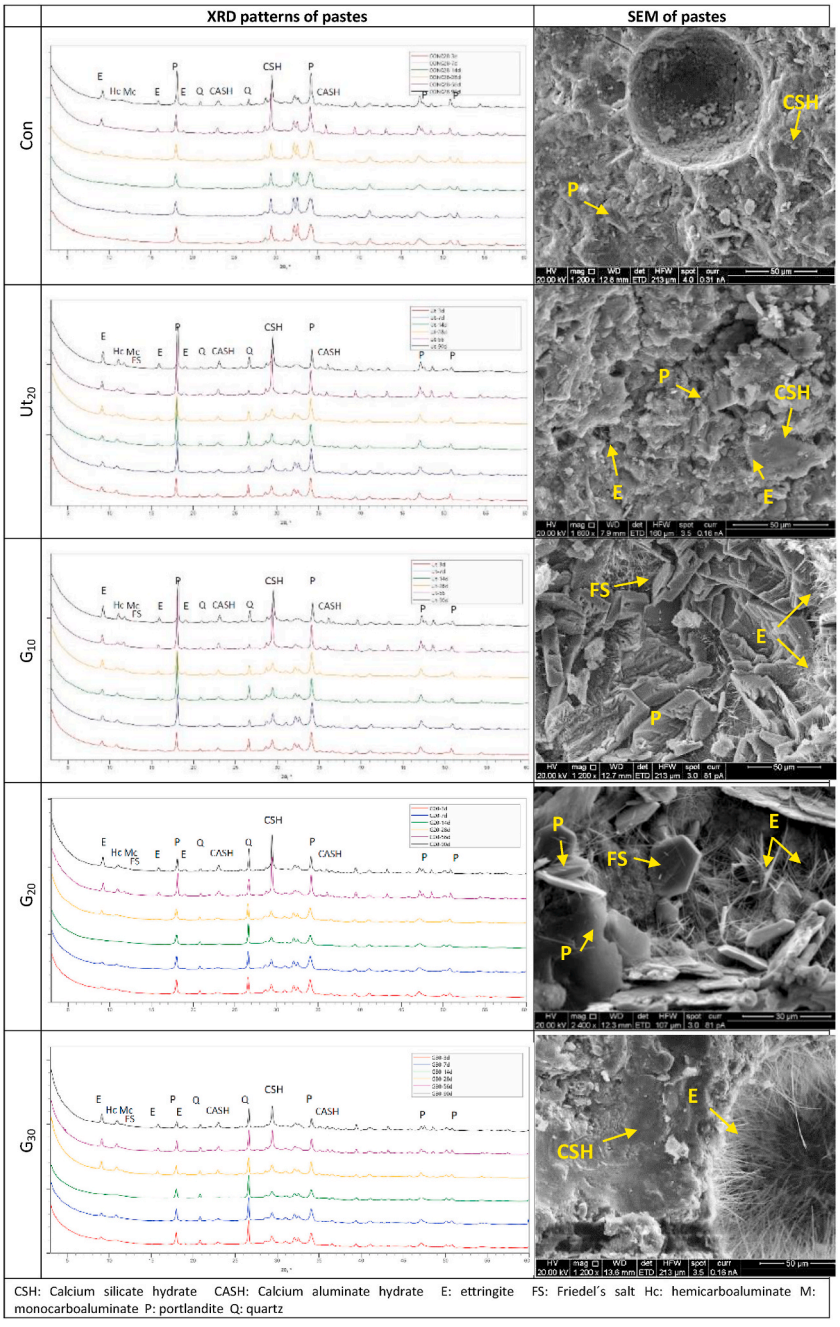

Fig. 12. Identification of hydration products by means of XRD.

that grinding, besides contributing to the formation of CSH and CASH as a result of the pozzolanic reaction, accelerates the formation of these compounds through the provision of additional nucleation sites. The presence of quartz (Q) is attributable to the quartz contained in ashes. SCBA contain higher amounts of gypsum, sodium, chlorides, magnesium and sulphates than sand, consequently, the formation of harmful compounds needs to be controled [45]. It can be observed that the addition of SCBA ashes promotes the formation of ettringite ($3CaO{\cdot}Al_2O_3{\cdot}3CaSO_4{\cdot}32H_2O$) through the reaction of the additional gypsum ($CaSO_4$) with calcium aluminate hydrates (C_3A and C_4AF). Ettringite (E) -AFt group-rapidly forms since early ages and observed up to 90 days being more significant in mixes containing Ut-SCBA, regardless incorporating the same amount of substitution rate as G_{20} specimens, meanwhile in the control specimens it is observable from 28d, Fig. 12. Well crystallised needled products are easily detectable in SEM images. Regardless the crystallinisation, the size and stability depends on the environment they form and grow [46]. In parallel, the formation of AFm-hemicarboaluminate (Hc) appears in pastes from early ages in all blended mixes and monocarbonates are clearly formed at 28d

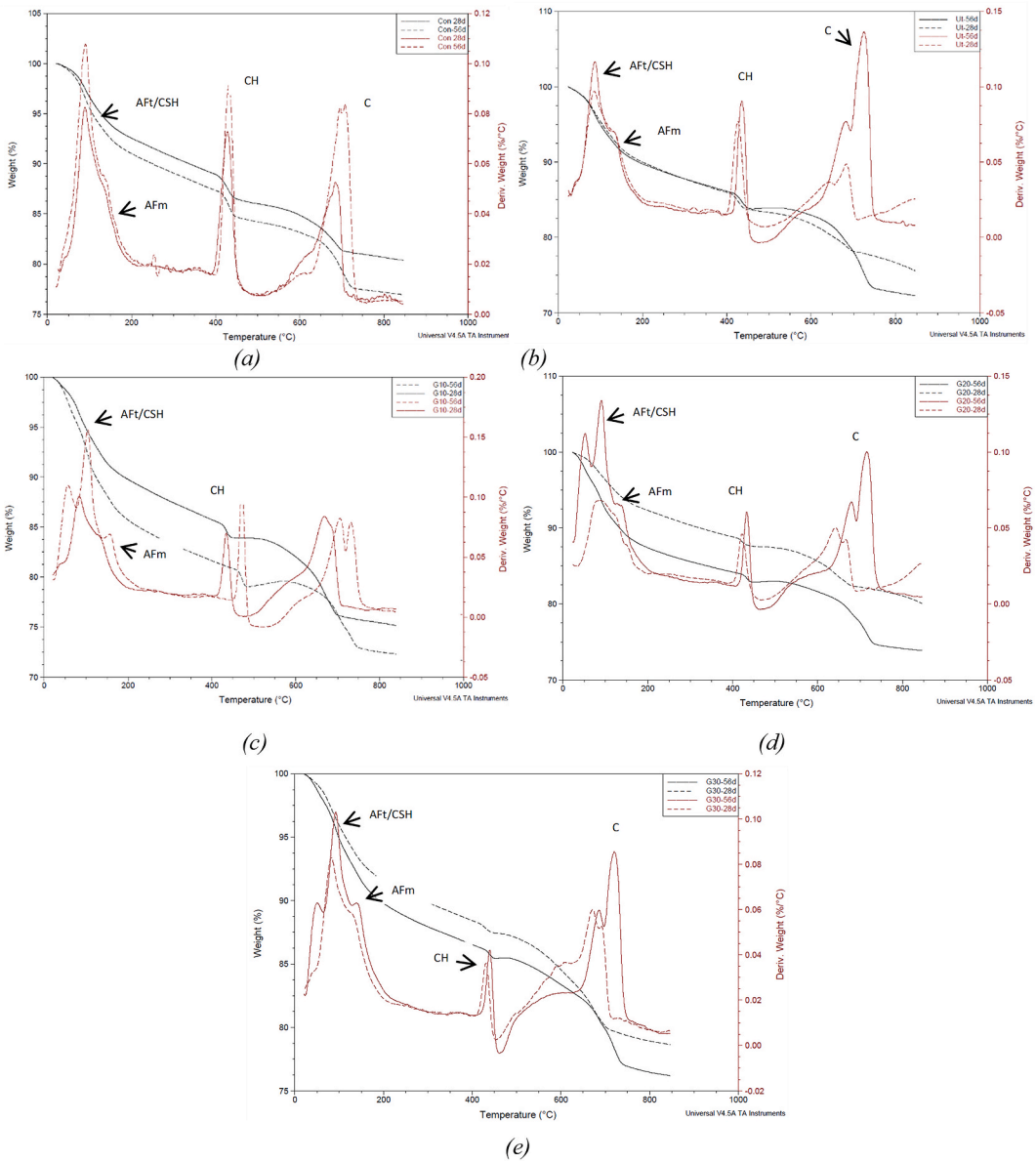

Fig. 13. Identification of hydration products by means of TGA-DTA.

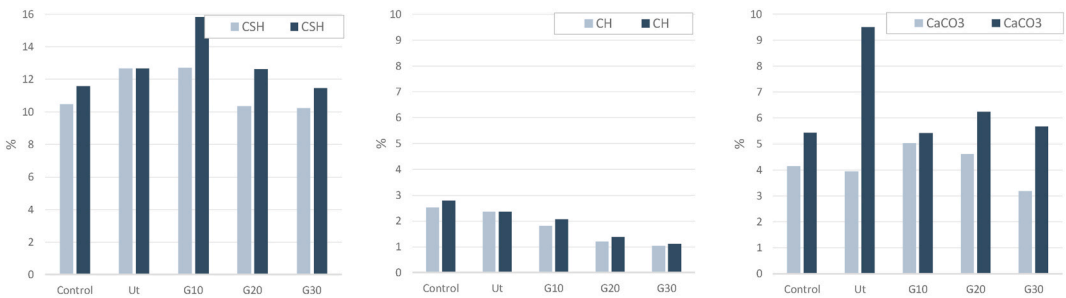

Fig. 14. Apparent quantification of CSH, CH and $CaCO_3$ by means of TG-DTA at 28 and 56d

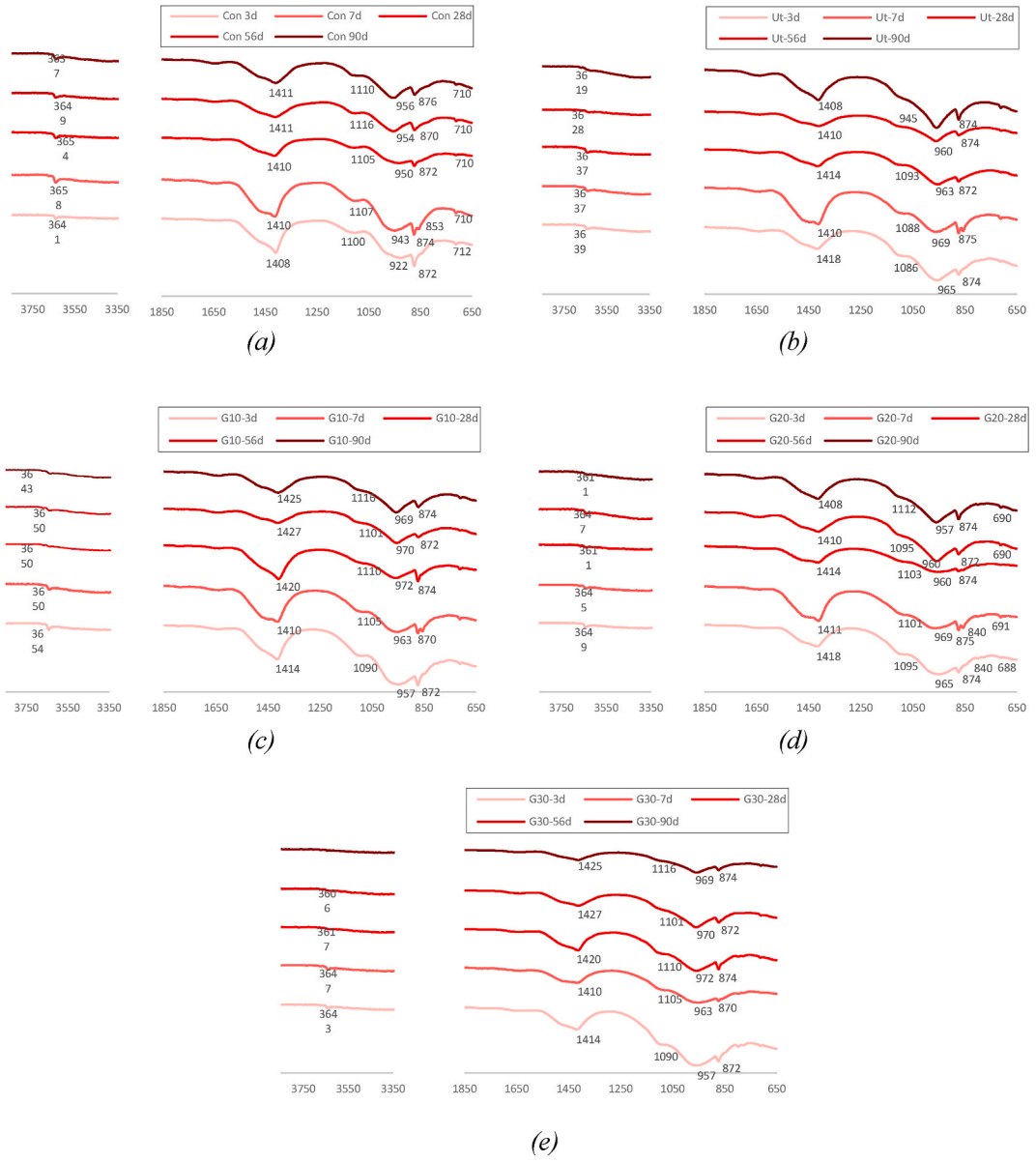

Fig. 15. FT IR spectra of Con, Ut_{20}, G_{10}, G_{20} and G_{30} at 3, 7, 28, 56 and 90d.

with higher intensity peaks in Ut-SCBA. The use of G-SCBA delays the formation of monocarbonates in pastes. This can be explained by the carbonation of pastes through which, due to the reaction with CO_2, the ettringite is prevented to convert into monosulfate which can lead to the formation of additional expansive ettringite [45]. Friedel's Salt (FS) was discretly observed by means of XRD and confirmed by means of SEM-EDS. FS formation correspons to the chemical binding of the admixed chlorides contained in the ashes by the chloride ions uptake capability of AFm hydrates. These compounds are expected to create more stable bonds than those that may form with entered chlorides. Other undesiderate products such as brucite ($Mg(OH)_2$) were not observed.

3.5.2. TGA

Powders from pastes cured for 28 and 56d were analysed by means of TGA-DTA, Fig. 13. Changes in mass loss due to the thermal decomposition (TGA) were then measured and attributed to the corresponding hydration product based on the ranges observed in DTA. Up to 105 °C, the mass loss is attributed to the unbound or weakly bound water. The weight loss occurring between 60 and 400 °C corresponds to the dehydration of CSH, AFt and AFm phases. The mass loss concentrated between 400 and 465 °C corresponds to the dehydroxilation of portlandite (CH) into CaO. The mass loss occurring at 630–800 is due to the decomposition of $CaCO_3$. The value of the ranges are approximately, since these swift to the right in the case of mixes containing ground ashes at 56d.

According to the TGA results, the addition of 10% of G-SCBA promotes higher amounts of CSH gel, either at 28d and 56d, Fig. 14.

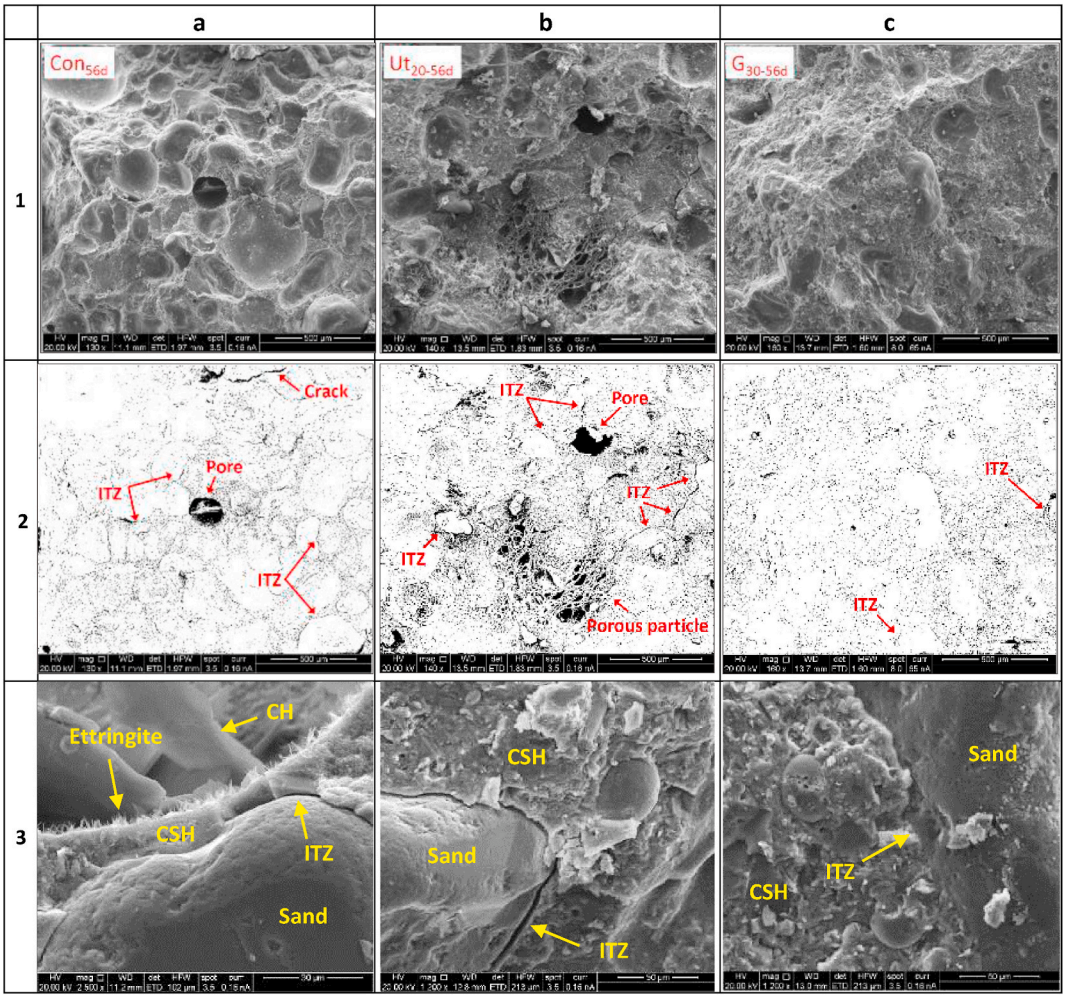

Fig. 16. Extent of the ITZ enhancement.

Based on TGA, Ut-SCBA and control samples would promote the formation of more quantity of CSH gel at 28d than G_{20} and G_{30}, regardless the observations made along this document. These discrepancies lie on the fact that CSH curve overlaps the curves of other hydration products such as AFt and free water, resulting in inaccurate results. On the other hand, the portlandite content decreases with the increase of substitution rate of ground ashes within the mix, that could be interpreted as a major consumption of CH in the pozzolanic reaction. Nevertheless, there are no direct correlations between the apparent production of CSH gel and the consumption of CH for pastes containing 20% and 30% of ground ashes. This is in agreement with the FTIR where the band at 960 cm^{-1} is less sharp for G_{30} than other mixes. This may demonstrate the existence of a limit substitution rate from which the system saturates and the hydration process is delayed. Additionally, future investigations on higher SR may consider the limited calcium content available for the pozzolanic reaction, thus, a portion of SCBA may remain unreacted.

The presence of $CaCO_3$ is due to the carbonation of the sample. The weight loss due to the decomposition of the calcium carbonate shows that untreated ashes promotes de carbonation of the samples, while by grinding this phenomenon is counteracted. This is attributable to the more porous structure of mortars and pastes containing Ut-SCBA that ease the diffusion of CO_2. Up to 28 days the higher the substitution rate of ground ashes, the lower the presence of $CaCO_3$. Nevertheless, at 56d all mixes containing ground ashes show similar rates of $CaCO_3$.

3.5.3. FTIR

FTIR spectra for Con, Ut_{20}, G_{10}, G_{20} and G_{30} at 3, 7, 28, 56 and 90 days are shown in Fig. 15. The O–C–O bands for carbonate phases appear in all spectra in the bands 1414–1427 and 870-876 cm^{-1}. The intensity is reduced, and the band becomes wider over time for all spectra up to 56d. After 90d, this is reverted potentially due to the carbonation process of samples that affect all samples but G_{30}. In this terms, Ut and G_{20} pastes seems to be more affected. This agrees with the results obtained in TGA for these samples. This is a matter of interest for future research to investigate the performance of these mixes in terms of carbonation resistance and carbon uptake.

The Si–O vibration bands at 3640 and 1091 cm^{-1} decrease along time corresponding with the consumption of $Ca(OH)_2$ during the

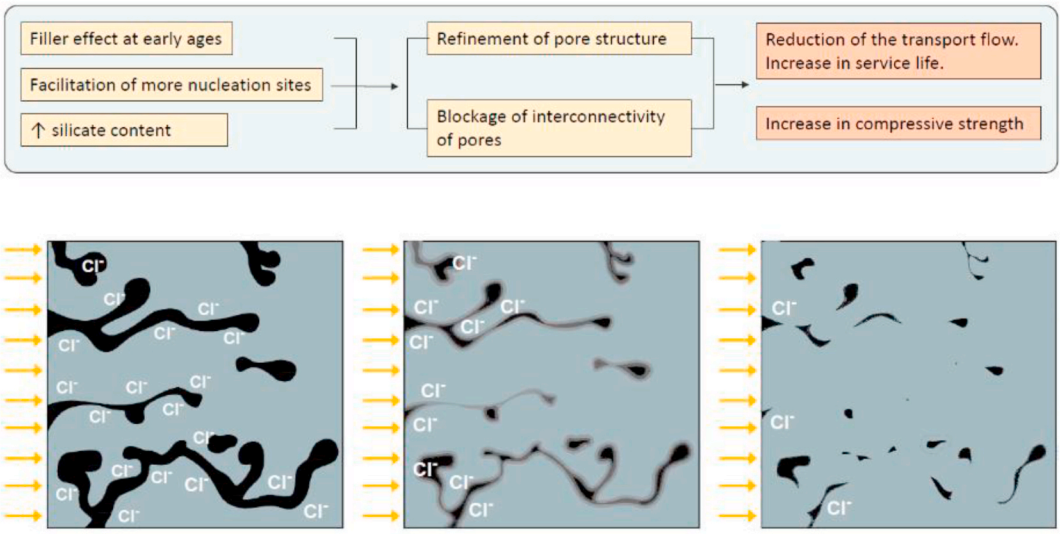

Fig. 17. Transport flow modifier mechanism promoted by G-SCBA in mortars.

pozzolanic reaction with amorphous SiO_2. The resulted CSH and CASH are observable at around 960 cm^{-1} (Si–O asymmetric stretching vibration) where bands are more intense and narrower with increased in curing age. The addition of treated and untreated SCBA makes the bands to shift to higher wave-number indicating a modification in the Ca/Si ratio as a result of the increasing polymerisation and the subsequent de-calcification process [47]. Nevertheless, after 28d the bands slightly shift to lower wave-number that may respond to the initial carbonation of samples that imply the decomposition of CSH gel in $CaCO_3$ and amorphous silica gel. In the case of Ut_{20}, this band increases after 28d and clearly increases at 90d confirming the existence of delayed pozzolanic reaction obtained from OP, (ρ_{sur}) and CS. These phases may hinder the existence of less representative AFt and AFm phases such as mono-carboaluminate, hemi-carboaluminate or stratlingite with medium intensity bands at 953-954cm-1 (Al–O) [47].

Unaltered vibration bands at 688-710 cm^{-1} correspond with crystalline quartz, also observable in non-blended samples. The O–H bands at 3658-3611 cm-1, noticed in all bands, is representative of portlandite which is clearly reduced over time in mixes containing SCBA. The band observed at around 1115 (S–O; $[SO4]^{2-}$) shows the existence of ettringite, observable in Con, G_{10}, G_{20} and G_{30} spectra. It can be notice that for all pastes the bands shifts towards higher wave-number along with curing age. In the case of untreated ashes this band is shifted to the right indicating the formation of less strong bonds.

3.6. Interfacial transition zone enhancement

The investigation of the interfacial transition zone (ITZ) between the fine aggregates and the cementitious paste showed the constant narrowing of gaps with measured widths at 56d of 0.89–1.14 μm, 2.58–3.28 μm, 0.26–1.24 μm, <0.29 μm for Con, Ut_{20}, G_{10}, G_{20} and G_{30} mixes respectively, Fig. 16. It has been observed by means of SEM that G-SCBA narrows and closes the interfacial transition zone (ITZ) between aggregates and the cementitious paste Fig. 16c. The ITZ has benefitted from the filling effect and the formation of secondary CSH gel resulted from the pozzolanic reaction. The enhanced bond between the fine aggregates and the paste, with greater intensity for G_{30} mixes at 28d and 56d, leads to further gains in compressive strength. These observations are in agreement to those from other authors [48,49] and could be attributed to additional portion of particles sizing below 1 μm provided by G-SCBA. The extent of the beneficial effect of G-SCBA was qualitatively explored by SEM and the photographic negative facilitated to ease its observation. Further research is desirable to characterise the extent, elastic properties and hardeness of the ITZ by using other methods such as SEM backscattered image analyses, 3D X-ray computed tomography [50,51] and by nanoindentation [52].

3.7. Mechanism of physico-mineralogical activation by grinding

The performance-based tests have demonstrated the capacity of ground ashes to physically modify the matrix by refining the pore structure over time, blocking the interconnectivity of pores, and filling the gaps in the ITZ between fine aggregates and paste. The refinement of the pore structure and blockage of channels were concluded based on CA, OP and ρ_{sur} tests. These along with the tracking of changes in the ITZ result in the high gains in compressive strength and the reduction in the transport flow observed by means of RCMT. Thus, mixes containing G-SCBA delays the time that chloride ions need to reach the critical chloride threshold for corrosion initiation, increasing the service life of RC structures. This is represented in Fig. 17.

However, it must be noted that, due to the rapid mechanisms induced by the electrical field, the binding of chlorides by the hydration products (out of the scope of this research) cannot occur, therefore in RCMT, this effect is disregarded which means that, the diffusion of chlorides can be still lower than considering only the transport mechanisms. The CBC can be physical or chemical and it is commonly attributed to the adsorption onto the surface of hydration products such as CSH -mainly- or Friedel's salt, and to the reaction between aluminates and chloride ions. The former is more prone to be released due to changes in the pore solution such as those

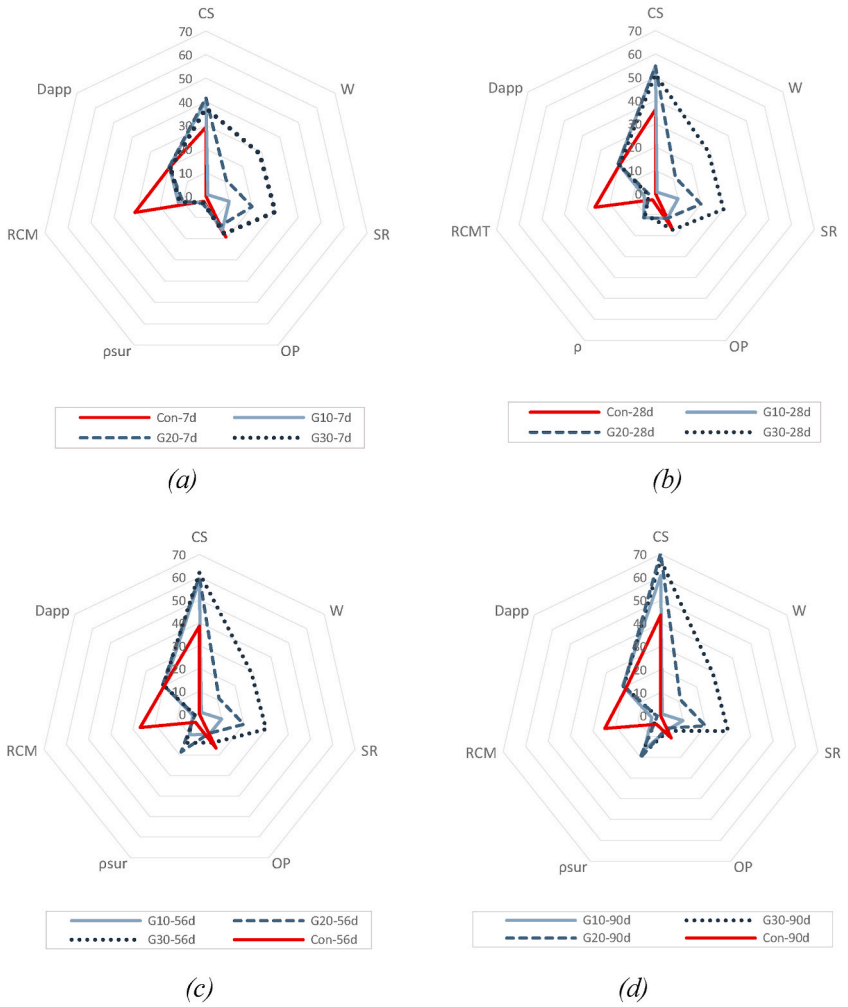

Fig. 18. Radial chart of Control, G_{10}, G_{20}, G_{30} specimens at a) 7 days, b) 28 days, c) 56 days and d) 90 days. CS: compressive strength (MPa); W: relative increase in casting water, (%); SR: substitution rate of fine aggregates by ashes (SR); OP: open porosity (%); ρ_{sur}: surface electrical resistivity (kOhm.cm); RCM: Rapid chloride migration coefficient (x10^{-12} m^2/s); D_{app}: apparent density (kg/m^3 x 10^{-2}).

Table 5
Performance of mortars at 28d when using different functional units: a) compressive strength and b) amount of ashes used.

	cem/CS (kg/MPa)	binder/CS (kg/MPa)	Fine agg./CS (kg/MPa)	Water/CS (l/MPa)	Dnssm/MPa
Con	16.80	0	50.39	8.40	0.763
G10	10.69	3.21	28.85	6.62	0.119
G20	10.02	6.01	24.05	5.55	0.044
G30	11.42	10.28	23.98	5.82	0.058

(*a*)

	cem/ash (kg/kg)	CS/binder (MPa/kg)	Fine agg./ash (kg/kg)	Water/ash (l/kg)	Dnssm/ash
Con	–	–	–	–	–
G10	3.33	0.31	9.00	2.06	0.037
G20	1.67	0.17	4.00	0.92	0.007
G30	1.11	0.10	2.33	0.57	0.006

occurring due to carbonation, while the later are more stable although can be also reversed in acidic environment [53,54]. Therefore, the use of SCBA as new mineral admixture can be beneficial in terms of CBC by supplying a higher amount of aluminates and silicates. Additional aluminates in SCBA can bind the chlorides within the ashes by forming FS as shown in Fig. 12, while still available

aluminates could react with entered chlorides. However, considering the production of CSH, physically adsorbed chlorides might be predominant in this type of mixes. Additionally, the char particles provided by Ut-SCBA are expected to have an additional adsorbent capacity for the chlorides [55].

The physical modification lies on the consumption of portlandite by the additional reactive SiO_2 promoting the generation of secondary CSH and CASH. At very early ages (1d and 3d) the lower results of ρ_{sur} obtained in G-specimens in contrast to the higher results for CS when compared to control specimens justify the initial filler effect of ground ashes.

The outperforming performance of G-SCBA in comparison to that of Ut-SCBA confirms the ability of grinding in providing more nucleation sites and, hence, promoting the mineralogical formation of CSH and CASH [44].

3.8. Optimum substitution rate

Fig. 18 shows the performance, the casting water in terms of relative increase and the substitution rate of control, G_{10}, G_{20}, G_{30} specimens at 7d, 28d, 56d and 90d. It can be easily observed the positive influence of G-SCBA in the CS development and the reduction in the diffusion of chlorides. On the other hand, the water demand can be pointed as the main drawback in the use of G-SCBA. Therefore, considering the enhanced durability performance and the highest compressive strength values, the amount of substitution rate and the water demand, G_{20} specimens result to be the optimum mix up to 90d.

This is a qualitative assessment that can vary according to the functional units (FU) assessed as shown in Table 5. A functional unit is a quantified description that enables the comparation of different systems. This is especially useful in life cycle assessment. For example, if considering the compressive strength of the material in MPa as a functional unit it can be seen how G_{20} is the mix that requires less amount of cement and water per MPa. It also halves the relative amount of aggregates equalling to that of G_{30}. The higher CS of G_{20}, enables getting thinner sections under same acting loads. However, if the amount of ashes is to be evaluated as the functional unit G_{30} gains interest. In both cases, the use on ground ashes reduces the use of natural resources and consequently, the overall energy associated to it and promotes the structural material minimization, both goals of the sustainable structural design [56].

4. Conclusions

This research investigates the use of sugarcane bagasse ash as high-performance fine aggregate for cementitious materials. For this purpose, ashes were treated by grinding, and the performance of mortars and pastes containing different substitution rates analysed and compared with samples containing untreated ashes and samples without ashes. A combination of analytical techniques was used to validate the performance-based experimental campaign results. Tests were carried out from 3 to 90 days. It can be concluded that:

- Ut-SCBA contain big porous particles that reduces the workability of mortars and increase the water demand (+68%), delivering more porous mortars. As a result, reductions in compressive strength of 52,5% at 28d were obtained.
- After the mechanical treatment, grinding, the water demand of Ut-SCBA has decreased by 34.5%.
- The incorporation of G-SCBA enhances the compressive strength of mortars up to 62% at 28d, decreases the porosity by 35%, highly improves the resistance to the diffusion of chlorides by 10 times and enhances the chloride electrical resistivity, up to 4 and 4.5 times at 28d in comparison to control specimens.
- G-SCBA improves the interfacial transition zone by narrowing and closing the gap between aggregates and pastes, potentially attributable to the higher supply of micro particles.
- The mechanisms behind the G-SCBA mechanical and durability performance are the refinement and blockage of the pore structure by the supply of more nucleation sites and the formation of secondary CSH and CASH.
- Grinding SCBA facilitates the use of higher amounts of industrial SCBA in the production of OPC systems. The optimum substitution rate at 28d was found to be 20% due to the increasing water demand with the SR. After 90d enhancements are still observed in all compositions containing SCBA, with major intensity in Ut_{20} and G_{30}.

G-SCBA can be used as mineral admixture in the production of cementitious materials able to increase the compressive strength and the chlorides penetration resistance extending the service life. It can be potentially also used in concrete production. This research finds a solution for ashes that are not suitable for cement substitution as per BS EN 450–1, and leverages the total mass of material, without producing further discards.

Authors Statement

The specific contributions made by each author are listed below: Veronica Torres de Sande: Conceptualisation, Methodology, Investigation, Writing – original draft and review & editing. Monower Sadique: Conceptualisation, Methodology, Writing – original draft and review & editing. Paloma Pineda: conceptualisation, Methodology, Writing – original draft and review. Ana Bras: reviewing, Writing – original draft

Declaration of competing interest

The authors declare that they have no known competing financial interests or personal relationships that could have appeared to influence the work reported in this paper.

Data availability

Data will be made available on request.

Acknowledgments

The authors of this paper wish to acknowledge the support of the LJMU for the fully funded PhD Scholarship to Veronica Torres de Sande and San Pedro Bioenergy for supplying the ashes.

References

[1] D.-Y. Oh, T. Noguchi, R. Kitagaki, W.-J. Park, CO2 emission reduction by reuse of building material waste in the Japanese cement industry, Renew. Sustain. Energy Rev. 38 (2014) 796–810.
[2] V. Beiser, The World in a Grain: the Story of Sand and How it Is Transformed Civilization, first ed. ed., Riverhead Books, 2018.
[3] WWF, in: L. Koehnken, M. Rintoul (Eds.), Impacts of Sand Mining on Ecosystem Structure, Process and Biodiversity in Rivers, 2018.
[4] U.N.E.P. Unep, Global Material Flows and Resource Productivity. Assessment Report for the UNEP International Resource Panel, 2016.
[5] OECD, HIGHLIGHTS Global Material Resources Outlook to 2060 – Economic Drivers and Environmental Consequences, 2019.
[6] F.a.A.O.o.t.U.N. FAO, FAOSTAT - Compared Data, 2020.
[7] V. Torres de Sande, M. Sadique, P. Pineda, A. Bras, W. Atherton, M. Riley, Potential use of sugar cane bagasse ash as sand replacement for durable concrete, J. Build. Eng. (2021), 102277.
[8] A. Sales, S.A. Lima, Use of Brazilian sugarcane bagasse ash in concrete as sand replacement, Waste Manag. 30 (6) (2010) 1114–1122.
[9] M. Zhao, Z. Han, C. Sheng, H. Wu, Characterization of residual carbon in fly ashes from power plants firing biomass, Energy Fuel. 27 (2) (2013) 898–907.
[10] British Standard Institution, BS EN 450-1:2012. Fly Ash for Concrete, Definition, specifications and conformity criteria, 2012.
[11] A. Rajasekar, K. Arunachalam, M. Kottaisamy, V. Saraswathy, Durability characteristics of Ultra High Strength Concrete with treated sugarcane bagasse ash, Construct. Build. Mater. 171 (2018) 350–356.
[12] R. Somna, C. Jaturapitakkul, P. Rattanachu, W. Chalee, Effect of ground bagasse ash on mechanical and durability properties of recycled aggregate concrete, Mater. Des. 36 (2012) 597–603 (1980-2015).
[13] N. Chusilp, C. Jaturapitakkul, K. Kiattikomol, Utilization of bagasse ash as a pozzolanic material in concrete, Construct. Build. Mater. 23 (11) (2009) 3352–3358.
[14] J.C. Arenas-Piedrahita, P. Montes-García, J.M. Mendoza-Rangel, H.Z. López Calvo, P.L. Valdez-Tamez, J. Martínez-Reyes, Mechanical and durability properties of mortars prepared with untreated sugarcane bagasse ash and untreated fly ash, Construct. Build. Mater. 105 (2016) 69–81.
[15] M.A. Maldonado-García, U.I. Hernández-Toledo, P. Montes-García, P.L. Valdez-Tamez, The influence of untreated sugarcane bagasse ash on the microstructural and mechanical properties of mortars, Mater. Construcción 68 (329) (2018).
[16] P.O. Modani, M.R. Vyawahare, Utilization of bagasse ash as a partial replacement of fine aggregate in concrete, Procedia Eng. 51 (2013) 25–29.
[17] P.C. Macedo, A.M. Pereira, J.L. Akasaki, C.F. Fioriti, J. Payá, J.L.P. Melges, Performance of mortars produced with the incorporation of sugar cane bagasse ash, Rev. Ingen. de Constr. 29 (2) (2014) 187–199.
[18] S. Ghannam, H. Najm, R. Vasconez, Experimental study of concrete made with granite and iron powders as partial replacement of sand, Sustain. Mater. Tech. 9 (2016) 1–9.
[19] A. Bahurudeen, D. Kanraj, V. Gokul Dev, M. Santhanam, Performance evaluation of sugarcane bagasse ash blended cement in concrete, Cement Concr. Compos. 59 (2015) 77–88.
[20] A. Rerkpiboon, W. Tangchirapat, C. Jaturapitakkul, Strength, chloride resistance, and expansion of concretes containing ground bagasse ash, Construct. Build. Mater. 101 (2015) 983–989.
[21] J.T. Kolawole, A.J. Babafemi, E. Fanijo, S. Chandra Paul, R. Combrinck, State-of-the-art review on the use of sugarcane bagasse ash in cementitious materials, Cement Concr. Compos. 118 (2021), 103975.
[22] S.-C. Pan, D.-H. Tseng, C.-C. Lee, C. Lee, Influence of the fineness of sewage sludge ash on the mortar properties, Cement Concr. Res. 33 (11) (2003) 1749–1754.
[23] G.C. Cordeiro, R.D. Toledo Filho, L.M. Tavares, E.M.R. Fairbairn, Pozzolanic activity and filler effect of sugar cane bagasse ash in Portland cement and lime mortars, Cement Concr. Compos. 30 (5) (2008) 410–418.
[24] G. Cordeiro, R. Toledo Filho, L. Tavares, E. Fairbairn, Ultrafine grinding of sugar cane bagasse ash for application as pozzolanic admixture in concrete, Cement Concr. Res. 39 (2009) 110–115.
[25] J. Payá, J. Monzó, M.V. Borrachero, M.M. Tashima, L. Soriano, 17 - bagasse ash, in: R. Siddique, P. Cachim (Eds.), Waste and Supplementary Cementitious Materials in Concrete, Woodhead Publishing, 2018, pp. 559–598.
[26] T. Murugesan, R. Vidjeapriya, A. Bahurudeen, Sugarcane bagasse ash-blended concrete for effective resource utilization between sugar and construction industries, Sugar Tech. 22 (5) (2020) 858–869.
[27] Bristish Standards Institution, BS EN 196-2:2013. Method of Testing Cement, Chemical analysis of cement, 2013.
[28] M. Fan, R. Brown, Comparison of the loss-on-ignition and thermogravimetric analysis techniques in measuring unburned carbon in coal fly ash, Fuel Energy Abstr. 43 (2001).
[29] G.C. Cordeiro, L.M. Tavares, R.D. Toledo Filho, Improved pozzolanic activity of sugar cane bagasse ash by selective grinding and classification, Cement Concr. Res. 89 (2016) 269–275.
[30] British Standard Institution, BI ISO 13320-1:2009. Particle Size Analysis, Laser diffraction methods, 2009.
[31] Bristish Standards Institution, BS EN 1097-6:2013. Tests for mechanical and physical properties of aggregates, Determin. part. dens. water absorp. (2013).
[32] b.S. Institution, BS EN 196-6:2018. Method of Testing Cement. Part 6: Determination of Fineness, 2018.
[33] B.S. Institution, BS EN 196-1:2016. Method of Testing Cement. Part 1: Determination of Strength, 2016.
[34] B.S. Institution, BS EN 1015-3:1999. Methods of Test for Mortar for Masonry. Part 3: Determination of Consistence of Fresh Mortar, 1999 (by flow table).
[35] B.S. Institution, BS EN 1015-6:1999. Methods of Test for Mortar for Masonry. Part 6: Determination of Bulk Density of Fresh Mortar, 1999.
[36] British Standard Institution, BS EN 1936: 2006. Natural Stone Test Methods. Determination of Real Density and Apparent Density, and of Total and Open Porosity, 2006.
[37] Bristish Standards Institution, BS EN 1015-18:2002. Methods of Test for Mortar for Masonry. Determination of Water Absorption Coefficient Due to Capillary Action of Hardened Mortar, 2002.
[38] NORDEST, NT BUILD 492. Concrete, Mortar and Cement-Based Repair Materials: Chloride Migration Coefficient from Non-steady-state Migration Experiments, 1999.
[39] M. Sadique, H. Al-Nageim, W. Atherton, L. Seton, N. Dempster, Analytical investigation of hydration mechanism of a non-Portland binder with waste paper sludge ash, Construct. Build. Mater. 211 (2019) 80–87.
[40] V.T.d.S.M.S.A.B.P. Pineda, Experimental techniques for assessing the chloride binding mechanisms in eco-efficient cement-based materials by using SCM: a critical analysis, J. xxxxxxxxxxxxxx (2021).
[41] P. Azarsa, R. Gupta, Electrical resistivity of concrete for durability evaluation: a review, Adv. Mater. Sci. Eng. 2017 (2017) 1–30.
[42] W. Morris, E.I. Moreno, A.A. Sagüés, Practical evaluation of resistivity of concrete in test cylinders using a Wenner array probe, Cement Concr. Res. 26 (12) (1996) 1779–1787.

[43] R. Yu, P. Spiesz, H.J.H. Brouwers, Effect of Nano-Silica on the Hydration and Microstructure Development of Ultra-high Performance Concrete (UHPC) with a Low Binder Amount, 2019.
[44] X. Ouyang, D.A. Koleva, G. Ye, K. van Breugel, Insights into the mechanisms of nucleation and growth of C–S–H on fillers, Mater. Struct. 50 (5) (2017) 213.
[45] P. Azarsa, R. Gupta, Electrical resistivity of concrete for durability evaluation: a review, Adv. Mater. Sci. Eng. 2017 (2017), 8453095.
[46] G. Paul, E. Boccaleri, L. Buzzi, F. Canonico, D. Gastaldi, Friedel's salt formation in sulfoaluminate cements: a combined XRD and 27Al MAS NMR study, Cement Concr. Res. 67 (2015) 93–102.
[47] M. Horgnies, J. Chen, C. Bouillon, Overview of the Use of Fourier Transformed Infrared Spectroscopy to Study Cementitious Materials, 2013.
[48] A. Joshaghani, M.A. Moeini, Evaluating the effects of sugar cane bagasse ash (SCBA) and nanosilica on the mechanical and durability properties of mortar, Construct. Build. Mater. 152 (2017) 818–831.
[49] A. Hussein, N. Shafiq, M. Nuruddin, F. Memon, Compressive strength and microstructure of sugar cane bagasse ash concrete, Res. J. Appl. Sci. Eng. Technol. 7 (2014) 2569–2577.
[50] J. Wang, A.P. Jivkov, Q.M. Li, D.L. Engelberg, Experimental and numerical investigation of mortar and ITZ parameters in meso-scale models of concrete, Theor. Appl. Fract. Mech. 109 (2020), 102722.
[51] P. Pineda, S. Medina-Carrasco, A. Iranzo, L. Borau, I. García-Jiménez, Pore structure and interdisciplinary analyses in Roman mortars: building techniques and durability factors identification, Construct. Build. Mater. 317 (2022), 125821.
[52] Y. Gao, C. Hu, Y. Zhang, Z. Li, J. Pan, Characterisation of the interfacial transition zone in mortars by nanoindentation and scanning electron microscope, Mag. Concr. Res. 70 (18) (2018) 965–972.
[53] H. Zibara, Binding of External Chlorides by Cement Pastes, 2001.
[54] L.-O. Nilsson, Overview of Prediction Models for Chloride Ingress into Concrete Structures, Nordic Mini Seminar & 1st, Göteborg, 2001 fib TG 5.5 meeting.
[55] V.A. Franco-Luján, M.A. Maldonado-García, J.M. Mendoza-Rangel, P. Montes-García, Chloride-induced reinforcing steel corrosion in ternary concretes containing fly ash and untreated sugarcane bagasse ash, Construct. Build. Mater. 198 (2019) 608–618.
[56] J.M. Danatzko, H. Sezen, Sustainable structural design methodologies, Pract. Period. Struct. Des. Construct. 16 (4) (2011) 186–190.